ISSN online 2545-2819
ISSN print 0800-6377

DOI: 10.2478/ncr-2025-0011

Received: March 28, 2025
Revision received: June 8, 2025
Accepted: June 10, 2025

Bending Stiffness of a Continuous Concrete Beam Post-tensioned with Unbonded Tendons

Tarja Nakari, M.Sc
Ph.D. student
Tampere University
Unit of Concrete and Bridge Structures
tarja.nakari@tuni.fi

Prof. Dr. Anssi Laaksonen
Tampere University
Unit of Concrete and Bridge Structures
anssi.laaksonen@tuni.fi

ABSTRACT
The ratio of bending stiffnesses at different critical points in the continuous prestressed concrete beam exerts an influence on the redistribution of internal forces, generally moment from support to field. The increasing load will result in the formation of a large number of cracks in the maximum moment regions. This, in turn, leads to a reduction of the flexural stiffness of the

member and finally the formation of plastic hinges. Four continuous two-span concrete beams prestressed with unbonded tendons were constructed and loaded up to failure at the laboratory of Civil Engineering in Tampere University. This article focuses on the examination of the flexural stiffness of the test beams during the loading tests. The average bending stiffness of the test beams, as determined through the measured deflections, was clearly less than the elastic value $E_{cm}I_g$, even at the low loading levels. The calculated rotation values in the centre support exhibited a good correlation with experimental results. However, these values remained below the observed values because, in the plastic hinge regions, the stiffness underwent a more rapid decrease. The total plastic rotation obtained from test results was approximately three times the plastic rotation capacity calculated using the Eurocode.

Key words: Flexural stiffness, bending stiffness, unbonded tendons, rotation capacity.

1. INTRODUCTION AND RESEARCH SIGNIFICANCE

The use of unbonded tendons in continuous concrete structures, such as beams and slabs, has become a common practice in the contemporary building industry. Concrete structures post-tensioned with unbonded tendons (UPC structures) provide an efficient and economical load-bearing system, enabling the reduction of cross-section dimensions and the augmentation of span lengths, thereby optimising structural efficiency and cost-effectiveness. The design of such structures is typically based on allowable stresses at service loads, while also meeting the requirements of ultimate limit state. The stress increase in the unbonded tendon due to external load after post-tensioning depends on the deformation of the entire structure. The principles of strain compatibility at the cross-section cannot be directly applied when the unbonded tendons are used. Achieving a strain that corresponds to a yield strain at failure in unbonded tendons is challenging due to the fact that the unbonded tendon stretches its entire length under increasing load. In the case of bonded tendons, the additional stress can develop when approaching the ultimate capacity. Consequently, UPC members exhibit distinct rigidity characteristics compared to bonded post-tensioned concrete members.

In the case of UPC beams, the application of an increasing load will result in the emergence of tensile stresses in the maximum moment regions, such as the centre support and mid-span regions. This will result in the formation of cracks in the aforementioned areas, which will consequently lead to a reduction in the bending stiffness of the member. The loss of bending stiffness in the beam will consequently influence the increase in deflections at an accelerating rate in accordance with the applied load. This, in turn, will affect the stress increase of the unbonded tendons. The ratio of bending stiffnesses at different critical points in the continuous beam exerts an influence on the redistribution of moment from support to span.

In 2012, Kim and Lee proposed a model to describe the flexural behaviour of a continuous unbonded post-tensioned member. This model incorporated the assumption of an idealised curvature distribution in the maximum moment region, building upon their previous studies. Their proposed expression employs the bending moment distribution and flexural stiffness ratio along the continuous member to reflect the effect of the loading type and moment redistribution [1]. Vu, Castel and François proposed a nonlinear finite element model for calculating the structural behaviour of post-tensioned prestressed beams with unbonded tendons [2]. The analysis model encompassed both the serviceability and ultimate states. The analyses were based on a macro finite element (MFE) model, in which the beam finite element is characterised mainly by its homogeneous average inertia. The analysis incorporates the concrete tension stiffening effect, the propagation of flexural cracks, and the additional lengthening of the unbonded prestressing tendons due to the applied load [2]. The experimental validation of the model was conducted using test beams of simple-span post-tensioned unbonded concrete beams. In addition, Lopes et al. proposed a numerical method for geometric and material nonlinear analysis of continuous UPC beams over the entire loading process up to failure [3]. The model includes the time-dependent behaviour of such beams under service conditions. The analysis demonstrates that the amount of non-prestressed steel significantly affects the behaviour of continuous beams, including the curvature, neutral axis depth, moment redistribution and time-dependent deformations [3]. Nonlinear finite element simulations of unbonded prestressed concrete beams under short-term loading were also presented by Sousa et. al [4] and Kang et al. [5].

Du et al. introduced a numerical method for the full-range analysis of unbonded prestressed concrete flexural members [6]. The analysis included the stress-path dependence of materials. The curvature ductility factors for members with bonded and unbonded tendons for given values of combined reinforcement index (CRI) were analysed and compared. The curvature ductility factor μ_ϕ was defined in the article as the ratio between the ultimate curvature ϕ_u and the curvature at first yield ϕ_y. It was observed that when the CRI was between 0.15 and 0.20, the ductility factor of an unbonded member was close to that of a bonded one. Conversely, at higher CRI values, the ductility factor of an unbonded member was higher than that of a bonded one, while at lower CRI values, the ductility factor of an unbonded member was lower than that of a bonded one. The parametric study was conducted only on simply supported rectangular beams [6]. In 2016, Du et al. presented a method to convert the cross-sectional area of unbonded prestressing tendons into the equivalent cross-sectional area of non-prestressed steel [7]. This can be used to determine the moment of inertia of cracked sections as well as Branson's effective moment of inertia in an unbonded post-tensioned continuous concrete beam [7,8]. The Branson's effective moment of inertia has been utilized subsequently in this study.

Terán-Torres et al. evaluated the relationship between the loss of stiffness of the cross-section and the determination of the crack width and the degree of cracking for the negative and positive moment zones, taking into account the relationship between adjacent spans, the magnitude of the loads, and the partial prestressing ratio [9]. A set of equations has been presented to determinate the stiffness factor (SF) and the crack width, which are employed to define the degree of deflection of continuous members and the degree of cracking. The flexural stiffness of the unbonded post-tensioned continuous member can be obtained by multiplying the stiffness factor (SF), the modulus of elasticity of the concrete, and the uncracked gross moment of inertia of the cross-section ($SF \cdot EI$) [9]. This can be used to determine the deflection.

Fu, Zhu and Wang proposed a method for assessing the stiffness which was based on the actual crack pattern [10]. The proposed method has been validated experimentally using a simply supported beam and four two-span continuous beams. The proposed method has been shown to correctly simulate the change in inertia, assess the beam stiffness and reflect the dependence of the stiffness on the crack pattern [10].

Four continuous two-span concrete beams, prestressed with unbonded tendons, were built and loaded up to failure at the laboratory of Civil Engineering in Tampere University. This article focuses on the examination of the bending stiffness of the test beams during the loading tests. The test results from the point of moment redistribution were partially published in 2024 [11] and from the point of tendon stress increase in 2025 [12]. The findings of the laboratory tests have been utilised in this study, and a comparison has been made between the test results and several calculation methods found in the literature, including the simplified method to estimate the rotation capacity of continuous beam according to Eurocode 1992-1-1 [13]. The objective of this study was to ascertain whether the structure develops sufficient cracks to cause significant plastic rotation even when it is subjected to torsional loading in addition to bending loads. Additionally, another objective was to find an analysis model that represents the reduction in flexural stiffness with the greatest possible precision.

2. EXPERIMENTAL PROGRAM

2.1 Description of test beams

In the Civil Engineering Laboratory of Tampere University, large-scale experimental loading tests were carried out on four continuous two-span concrete beams and loaded to failure (Figure 1). The beams were post-tensioned with eight unbonded mono-strands with a symmetrical tendon profile consist of parabolic segments. The test beams had two equal spans of 10 m. The dimensions and reinforcement arrangement of the T-shaped test beams are shown in Figure 2 and summarised in Table 1 [11].

Table 1 – Reinforcement of test beams [11]

Test beam	As1 (mm^2)	As2 (mm^2)	As3 (mm^2)	As4 (mm^2)	As5 (mm^2)	Stirrups H1 (#12)	Flange stirrups H2 (#12, 2-par bundles)
B1	628 (2#16 + 2#12)	452 (4#12)	678 (6#12)	678 (6#12)	0	198 pcs c/c 100 mm	198 pcs c/c 100 mm
B2	628 (2#16 + 2#12)	452 (4#12)	678 (6#12)	1357 (12#12)	0	198 pcs c/c 100 mm	198 pcs c/c 100 mm
B3	628 (2#16 + 2#12)	452 (4#12)	678 (6#12)	1357 (12#12)	678 (6#12)	198 pcs c/c 100 mm	198 pcs c/c 100 mm
B4	628 (2#16 + 2#12)	452 (4#12)	678 (6#12)	1357 (12#12)	0	208 pcs c/c 75 mm /100 mm	198 pcs c/c 100 mm

Figure 1 – Test arrangement in the laboratory [11].

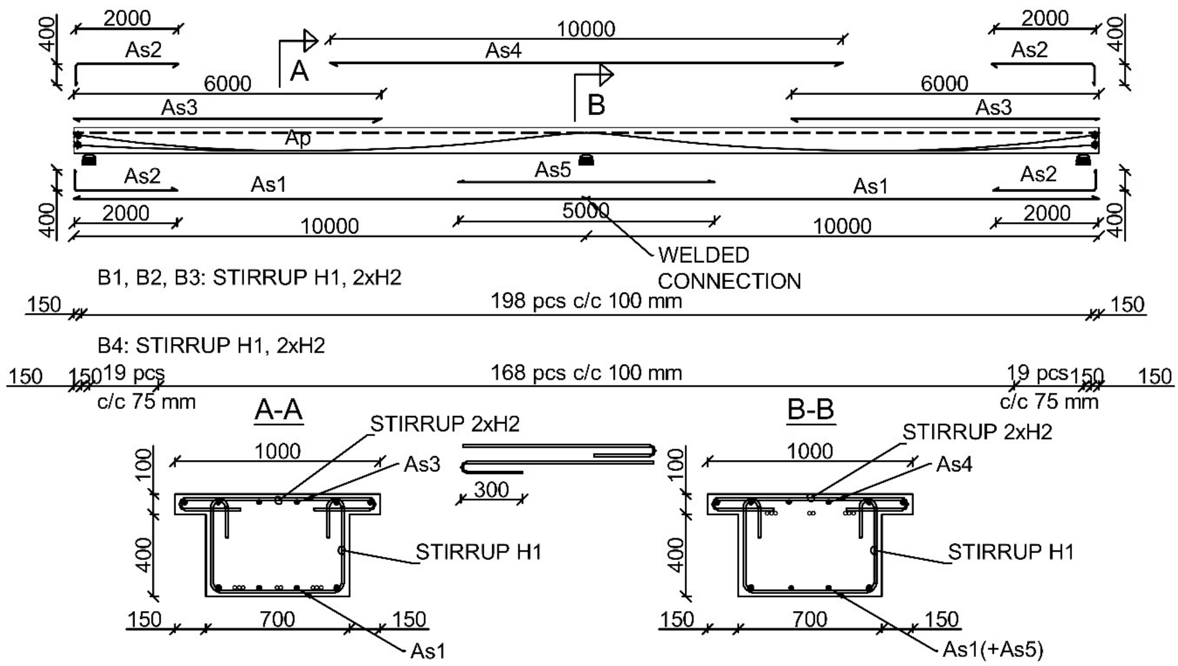

Figure 2 - Reinforcement arrangement of test beams [11].

At the centre support section, the amount of non-prestressed steel varied between the test beams, otherwise the reinforcement arrangement was kept constant in all the test beams. In beam B1, the amount of non-prestressed longitudinal reinforcement was equal to the minimum area of bonded reinforcement required by Eurocode EN 1992-1-1 [13] at both the centre support and the mid-span. For the other test beams, the tension reinforcement of the centre support was doubled. In beam B3, six compression reinforcement bars were added to the compression zone in the centre support. The stirrup spacing was maintained at a constant interval of 100 mm, except at the ends of the beam B4, where the spacing was reduced to 75 mm. A relatively high shear reinforcement ratio was used to prevent shear failure during the loading tests. Additional stirrups were also included in the anchorage zones of the unbonded tendons to resist the local crushing and transverse tension forces. The thickness of the concrete cover was 20 mm [11].

The designed concrete class was C30/37 according to Eurocode EN 1992-1-1 [11,13]. The average concrete cylinder strength varied between 38 and 43 MPa according to the compression tests of test cylinders (d = 150 mm and h = 300 mm) cast from the batches of each test beam. Table 2 gives details of the properties of prestressing and non-prestressing reinforcement [12].

Table 2 - Reinforcement material properties [12]

Type of reinforcement	**Area [mm^2]**	**Modulus of elasticity E_s [GPa]**	**Yield strength f_y or $f_{p0.1k}$ [MPa]**	**Tensile strength/ upper yield strength R_m/R_{eH} [MPa]**	**Elongation at maximum force A_{gt} [%]**
B500B T12	113	200	500	550	5
B500B T16	201	200	500	550	5
Y1860S7-15.7	149.55	201.7	1693	1883	4.8

2.2 Instrumentation

Strain gauges (SGB) were used to measure the strains in the non-prestressed rebars. These gauges were attached to the top and bottom longitudinal rebars and to the stirrups near the centre support. The measurement instrumentation recorded the strains in the reinforcement bars during prestressing and the load test. The strains on the different surfaces of the test beams were measured using the displacement gauges (LVDT). These were mainly installed after prestressing, so they only recorded deformations during the load test [11]. In addition, the displacement gauges were used to measure a rotation of the support area and the deflection of the test beam during prestressing and the loading. The detailed locations of the sensors are shown in Figure 3 [11].

Force sensors were used to measure the force in the unbonded strands from both anchors of two tendons in each test beam. The tendon force was measured both during tendon prestressing and during the load test. The results from these sensors are presented in more detail in the author's article published in 2025 [12].

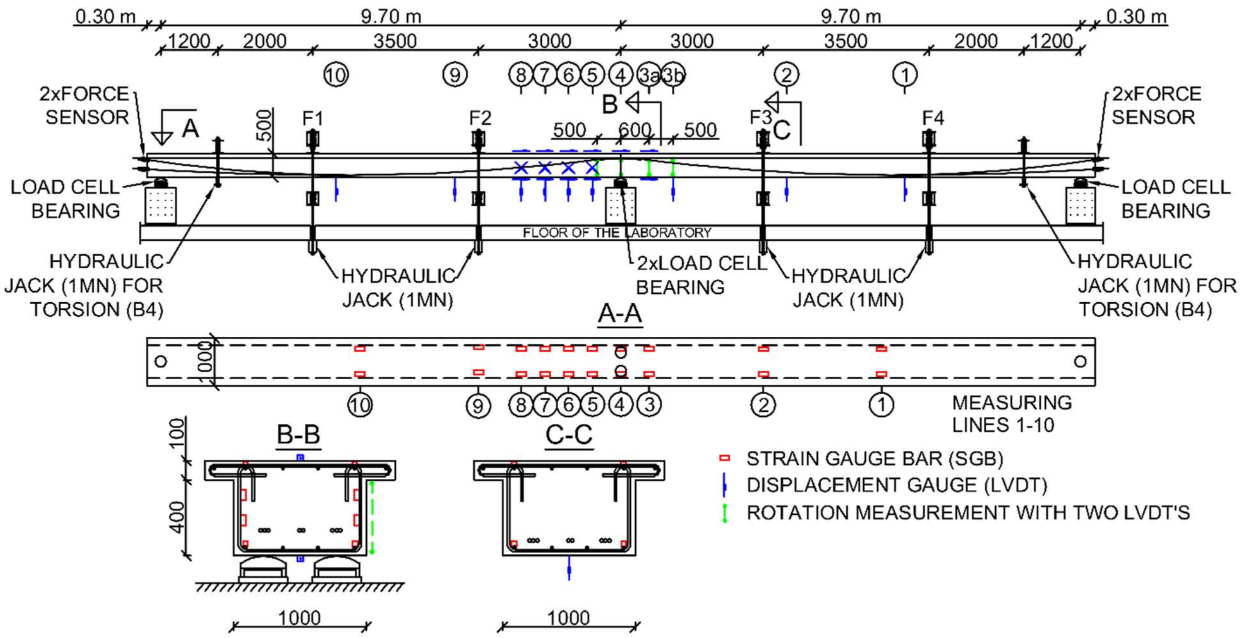

Figure 3 - Test setup and instrumentation [11].

2.3 Test setup in the laboratory

The test beam was first lifted onto the supports via four lifting points and then the strands were post-tensioned at the final load test position. An additional support was added at the midpoint of each span, which was later removed after prestressing. During the post-tensioning phase, the beam was supported at five points. The remaining measuring and loading arrangements were installed after the mono-strands had been post-tensioned. Loading was applied with two point loads on each span, located approximately one third of the span length from the support. Four 1000 kN force-controlled hydraulic jacks were used to apply the point loads. Steel frames were used to transmit the load from the hydraulic jacks to the beam. All test beams were subjected to bending loading but beam B4 was subjected to torsional loading in addition to bending loading. [11]

The test beams were supported by single bearings located under the beams at both ends of the test beams. These allowed for longitudinal displacement and rotations around all axes. The centre support had two bearings side by side, which allowed for rotation in the main direction but not around the beam longitudinal axis. All bearings were fitted with force sensors to measure the reaction of the support at different stages of the test. During loading of the B4 test beam, the hydraulic torsion jacks were positioned 1.2 metres from each end support of the beam [11].

A loading programme was prepared for each test beam. It started with four repeated loading steps at the low load level corresponding to the serviceability limit state according to Structural Eurocodes EN 1990 [14]. After each of these loading steps, the load was removed. Then the loads in the hydraulic jacks were increased until the maximum deflection capacity of the test setup was reached. After each load step, visible cracks were highlighted with a marker pen and the crack width of a few selected cracks was measured with a crack measuring loupe. For safety reasons, this was continued slightly below the level where the capacity of the test beam was reached, as determined by Eurocode EN 1992-1-1 [13].

3. FLEXURAL STIFFNESS

3.1 Bending stiffness EI

The secant modulus of elasticity of concrete E_{cm} for each test beam has been calculated in accordance with Eurocode 1992-1-1, utilising the actual concrete strength of each beam as determined during the load tests. The uncracked gross moment of inertia of the concrete cross-section I_g has been evaluated over the span of the test beams, thereby accounting for both the concrete cross-section and non-prestressed reinforcement in that section. The mid-span sectional properties were used in the analysis because the rigidity of the mid-span has a predominant effect on the deflections. These values have been collected in Table 3.

When cracks occur in the most stressed areas of the UPC beam, the cracked moment of inertia I_{cr} should be utilised for the section of cracked areas while the gross moment of inertia I_g should be used for the uncracked sections. This method is difficult and impractical to apply in this study, where the cracked areas expanded with increasing load. The actual stiffness of the beam lies between $E_{cm}I_g$ and $E_{cm}I_{cr}$, depending on the extent of cracking and the contribution of the concrete between the cracks to the tension. Consequently, the effective moment of inertia I_e developed by Branson [8] and the equivalent cross-sectional area A_{pe} of non-prestressed steel according to Du et al. [7] were also included in this study. The unbonded prestressing steel can be transformed into the equivalent cross-sectional area A_{pe} of non-prestressed steel by equation

$$A_{pe} = \frac{A_p \sigma_{pe}}{f_y} \tag{1}$$

where A_p is the cross-sectional area of unbonded tendons, σ_{pe} is the effective prestress in unbonded tendons and f_y is the yield stress of non-prestressed steel. The effective prestress of the test beam B1 was 961 MPa, in beam B2 835 MPa, in beam B3 816 MPa and in beam B4 834 MPa [12]. The neutral axis depth c will coincide with the depth of compression zone y at the fully cracked state. The depth of compression zone y in a fully cracked UPC T-section can be determined by basic structural mechanics as (shown in Figure 4)

$$\frac{1}{2}by^2 - \frac{1}{2}(b - b_w)\left(y - h_f\right)^2 + n_s A_{sc}(y - d_{sc}) = n_s A_s(d_s - y) + n_p A_{pe}\left(d_p - y\right) \tag{2}$$

where modular ratio for non-prestressing steel is $n_s = E_s/E_c$ and for prestressing steel $n_p = E_p/E_c$, h_f is the thickness of the flange, b_w is the width of the web, b is the width of the flange, A_s and A_{sc} are the areas of tension and compression non-prestressed reinforcement and d_s, d_{sc} and d_p are the effective depth of the non-prestressed steel and the prestressed steel, respectively. It is assumed that y is greater than the thickness of the flange h_f. For rectangular sections and flanged sections where y does not exceed the thickness of the flange, b_w is equivalent than b. The moment of inertia I_{cr} can then be determined by the following equation

$$I_{cr} = \frac{1}{3}by^3 - \frac{1}{3}(b - b_w)\left(y - h_f\right)^3 + n_s A_s(d_s - y)^2 + n_s A_{sc}(y - d_{sc})^2 + n_p A_{pe}\left(d_p - y\right)^2 \tag{3}$$

The effective moment of inertia I_e can then be calculated from equation [8]

$$I_e = (\frac{M_{cr}}{M_n})^3 I_g + [1 - (\frac{M_{cr}}{M_n})^3] I_{cr} \leq I_g \tag{4}$$

where M_{cr} and M_n are the cracking and total applied moment at the critical section of the beam, respectively. The values of bending stiffness of the test beams by using the effective moment of inertia were collected to Table 3.

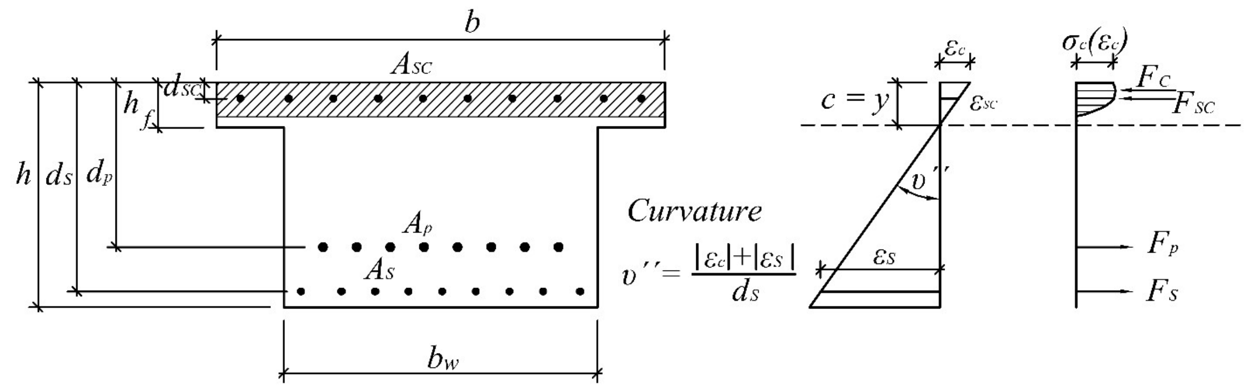

Figure 4 – Stresses, strains and internal forces of a fully cracked section.

Additionally, the bending stiffness of the test beams was determined experimentally, utilising the deflection values obtained from the displacement sensors and the load values applied by the hydraulic jacks.

The deflection at the measurement points 1 and 10 is obtained by the superposition principle as the sum of the elastic lines caused by the point loads acting in each span and the support moment with an assumption of the constant *EI*, as demonstrated in Figure 5. The measurement points 1 and 10 are both situated at a distance of 3.7 meters from the edge supports (A and C). The deflection of the point loads F_1 to F_4 at point x is thus obtained by the following formula

$$\upsilon_x = \frac{F}{6LEI}[ab(L+b)x - bx^3 + L < x-a >^3] \tag{5}$$

$$< x-a >^n = \begin{cases} (x-a)^n & if\ x-a \geq 0 \\ 0 & if\ x-a < 0 \end{cases}$$

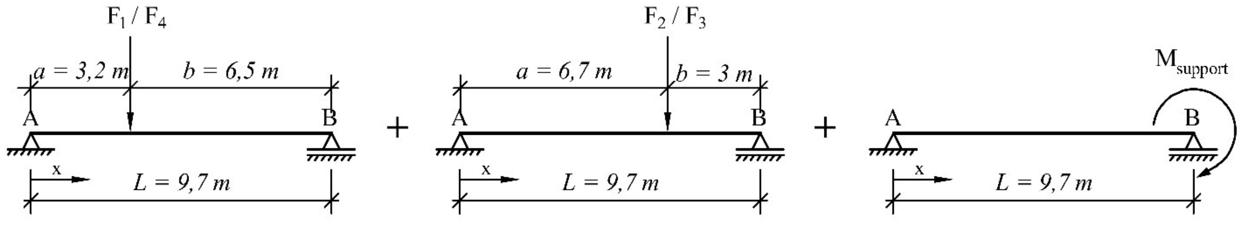

Figure 5 – Determination of deflection by superposition principle.

The deflection at point x, caused by the bending moment at the centre support, is obtained by the equation

$$\upsilon_x = \frac{M_{support}}{6LEI}(L^2x - x^3) \tag{6}$$

Using the measured deflection values at the measuring points 1 and 10 (υ_1 and υ_{10}) and the support moment value determined from the test results, the following equations are obtained for the bending stiffness of the test beams.

$$(EI)_{10} = \frac{1}{\upsilon_{10}}\left(\frac{918.72}{58.2}F_1 + \frac{792.54}{58.2}F_2 - \frac{297.48}{58.2}M_{support}\right) \tag{7}$$

$$(EI)_1 = \frac{1}{\upsilon_1}\left(\frac{918.72}{58.2}F_4 + \frac{792.54}{58.2}F_3 - \frac{297.48}{58.2}M_{support}\right) \tag{8}$$

The value of the bending stiffness is determined as the average of the values of both spans. The value examined at the lowest load level, where the beam could be assumed to still act almost elastically, are summarized to the last column in Table 3. The same method has also been used to calculate values for other load levels, up to the level at which the maximum measured deflection value was reached. These other values from both spans of each test beams in the different load steps can be seen in Figure 7.

Table 3 - Bending stiffness values of the test beams

Test beam	Average concrete strength at time of loading [MPa]	Secant modulus of elasticity E_{cm} [MPa]	Moment of inertia uncracked section I_g [m^4]	Elastic bending stiffness $E_{cm}I_g$ [MNm^2]	Moment of inertia fully cracked section I_{cr} [m^4]	Effective moment of inertia I_e [m^4]	Effective bending stiffness $E_{cm}I_e$ [MNm^2]	Bending stiffness determined from test results at first load step $E_{cm}I$ [MNm^2]
B1	39	34999	0.00869	**304**	0.00243	0.00264	**93**	**195**
B2	43	35972	0.00869	**312**	0.00217	0.00235	**84**	**197**
B3	38	34774	0.00870	**302**	0.00221	0.00230	**80**	**196**
B4	39	34999	0.00869	**304**	0.00222	0.00244	**85**	**183**

Terán-Torres et al. introduced an equation to determine a stiffness factor (SF) for partially post-tensioned members with unbonded tendons [9].

$$SF = \left[1 - \left(\frac{M_a - M_{cr}}{M_n - M_{cr}}\right)\left(1 - \frac{I_{cr}}{I_g}\right)\right] \tag{9}$$

where M_a is an acting moment at the different loading stage, M_{cr} is the cracking moment, M_n is the bending momentcapacity, I_g is the gross moment of inertia of the uncracked cross-section and I_{cr} is the moment of inertia of the fully cracked section. The bending stiffness of the member at the different load steps can then be achieved as a multiplication of the stiffness factor and the elastic bending stiffness ($SF \cdot E_{cm}I_g$). The calculated stiffness factors of the test beams are shown in Figure 6.

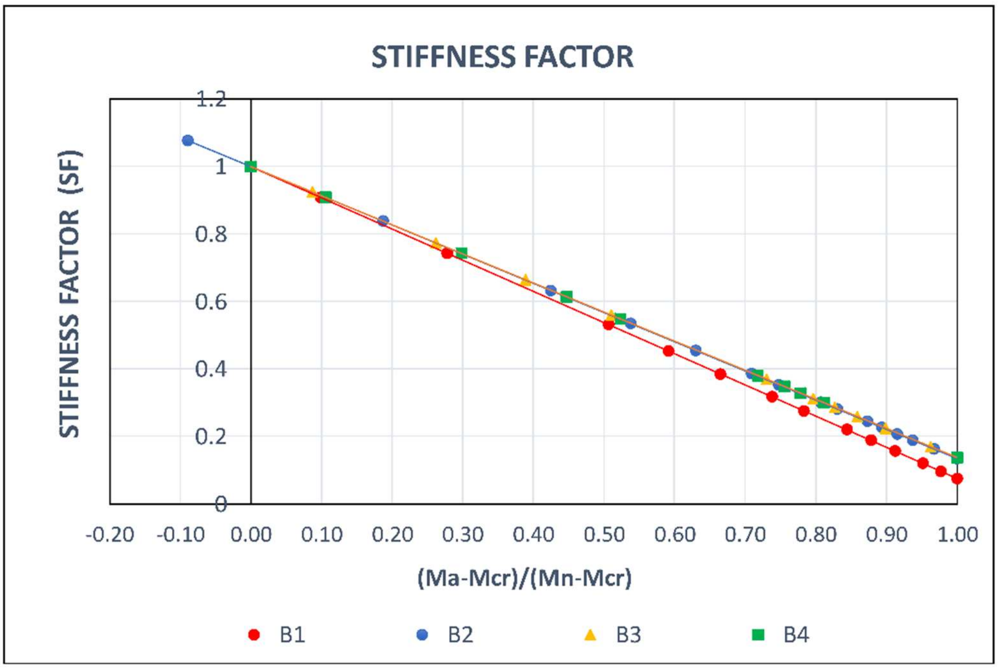

Figure 6 – Stiffness factor.

The bending stiffness values of the test beams as determined by the aforementioned methods are illustrated in Figure 7. At the point of failure, the calculated bending stiffness, derived from the actual deflections, and the bending stiffness calculated using the stiffness factor (SF) are found to reach approximately the same value. The constant values for the elastic bending stiffness and the effective bending stiffness are illustrated as horizontal lines in Figure 7. It is important to note that the calculated stiffness values (red and blue lines) are determined on the basis of deflection measurements, and thus represent experimental results.

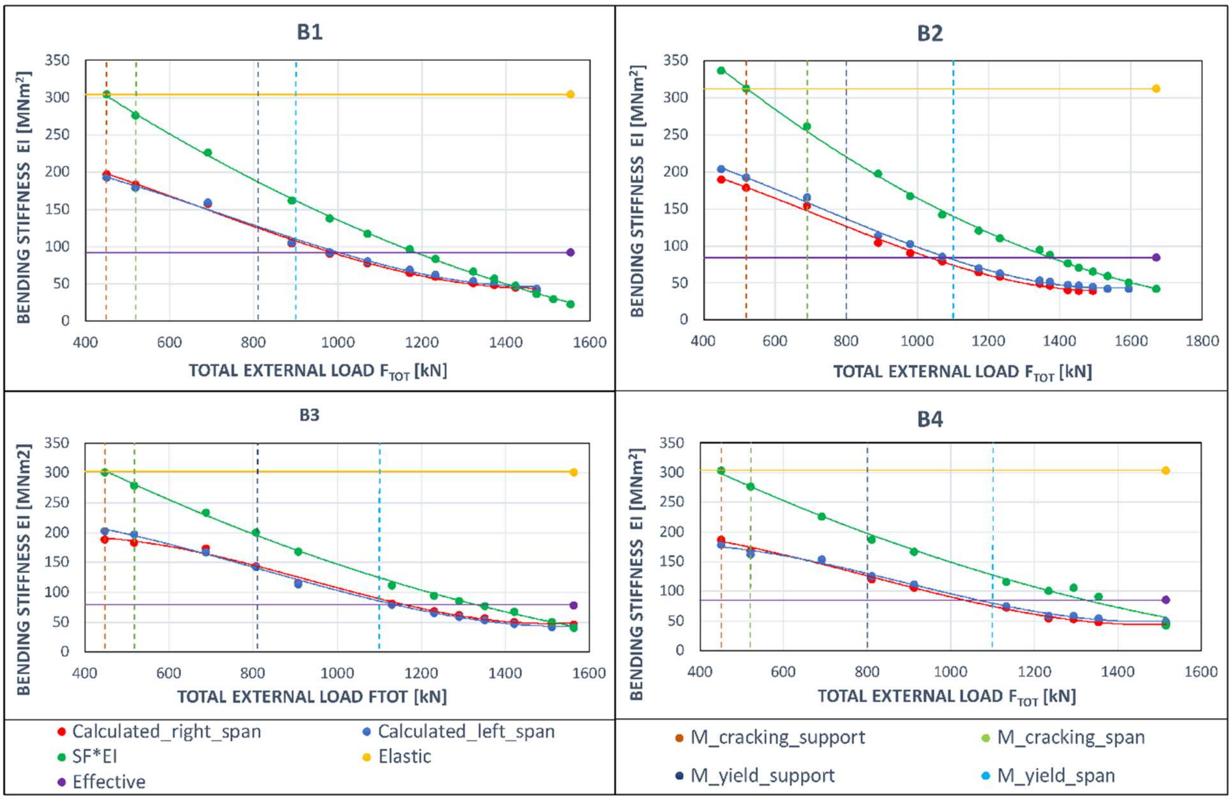

Figure 7 - Bending stiffness values of the test beams.

3.2 Rotation of the centre support area

The rotation of the centre support was calculated for the two-span continuous test beams by several different methods. In a similar manner to the deflection described above, the rotation of a hyperstatic beam at a centre support is also obtained using the superposition principle. The rotation of the centre support from the point loads F_1 to F_4 at point x is thus obtained by the following formula

$$\upsilon'_x = \frac{-Fab(L+b)}{6LEI} \tag{10}$$

Similarly, the rotation of the centre support, caused by negative bending moment at the centre support, is obtained by the equation

$$\upsilon'_x = -\frac{M_{support}L}{3EI} \tag{11}$$

The total rotation on both side of the centre support is obtained by entering the beam length and distances between the loads into the relevant equations.

$$\upsilon'_{(10)} = \frac{1}{EI}\left(\frac{268.32}{58.2}F_1 + \frac{329.64}{58.2}F_2 - \frac{9.7}{3}M_{support}\right) \tag{12}$$

$$v'_{(1)} = \frac{1}{EI}\left(\frac{268.32}{58.2}F_4 + \frac{329.64}{58.2}F_3 - \frac{9.7}{3}M_{support}\right) \tag{13}$$

The following analysis examined the total rotation of the central support area, i.e. the sum of the rotations calculated using Equations 12 and 13. The analyses utilized the values presented in the previous chapter for the bending stiffness of the test beams (*EI*), namely the elastic bending stiffness, the effective bending stiffness, and the bending stiffness calculated from the measured deflection of the test beams and varying according to load levels. The support moment value calculated from the test results using loads and support reactions was used for the support moment $M_{support}$. The analysis does not include the beam's own weight or secondary moments. This is because the displacement and deflection sensors were not installed until after the tendons had been post-tensioned.

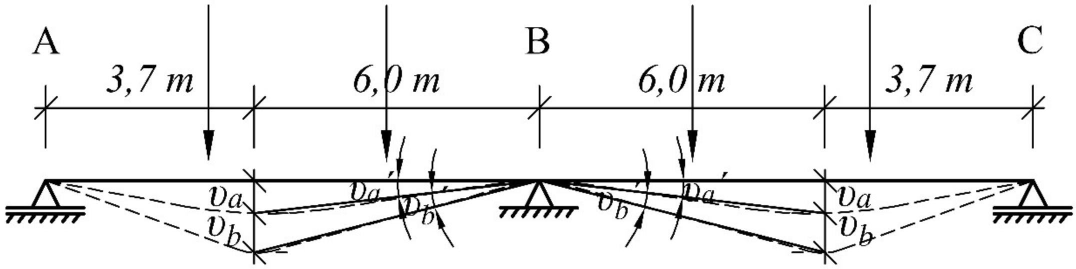

Figure 8 – An alternative calculation method (D).

An alternative calculation method (marked with the letter D in the following Chapter) was employed in the computational analyses. In this method, a value for the rotation (v_a') of the centre support is calculated for each load step using the constant value of the bending stiffness of the first load step, $E_{cm}I$ (last column of Table 3). This results in a mid-span deflection v_a, which is mainly smaller than the measured total deflection v_1 *or* v_{10} from the same point. The difference between these two deflections is the additional deflection v_b. The additional rotation (v_b') at the centre support corresponding to this additional deflection v_2 is obtained by means of trigonometry, as illustrated in Figure 8. The total rotation of the centre support v_{tot}' is then obtained from the equation

$$v'_{tot} = 2 \cdot (v'_a + v'_b\ ) \tag{14}$$

The efficacy of the method is optimised when the shape of the deflection line approximates a fracture line more closely than it does a continuous parabolic deflection line.

Displacement gauges were utilised to quantify the rotation of the centre support area, as shown in Figure 9. [12]. The rotation measurements were positioned on either side of the centre support, one 500 mm from the centre support, the second 600 mm and the third 1100 mm from the support. The locations of the measurement points are shown in green in Figure 3 [11]. The rotation results of the centre support were calculated as the sum of the results of the measuring points on either side of the support. The distance between these points was 900 mm, approximately twice the effective height d [12].

Figure 9 – Rotation measurement at the centre support.

The rotation was also calculated using the curvature of the beam's support area. The value of the curvature at different load levels was calculated from the results of the strain gauges on the top and bottom reinforcement of the test beam. On some of the test beams, these strain gauges at the top of the centre support were damaged during the load test and no results were obtained from them at high loading levels. In these cases, the values from the displacement gauges on the top surface of the beams were used. Rotation can be estimated by multiplying the curvature by the plastic hinge length of the support area.

$$v'_{tot} = v'' \cdot l_p \tag{15}$$

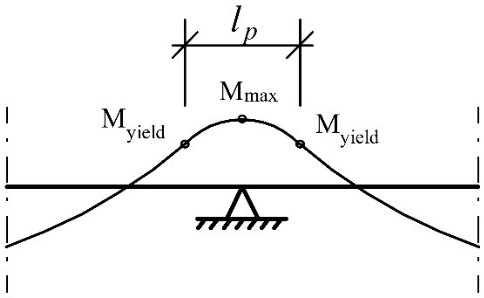

Figure 10 – The length of the plastic hinge.

The length of the plastic hinge l_p is defined as the distance at which the non-prestressed top reinforcement in the support area has yielded under the maximum load of the load test, shown in Figure 10. The non-prestressed reinforcement did not yield at the measuring points 3 and 5 at failure. These points were located 600 mm from the centre support on both sides of the support. Therefore, the length of the plastic hinge must be less than 1.2 meters. However, no strain gauges had been attached to the top reinforcement between these points and the centre point (point 4), and no strain results from that distance were recorded. The value 600 mm ($2 \cdot 0{,}6 \cdot h$) for the plastic hinge length was adopted from Eurocode 1992-1-1 [13] and used in the calculation.

3.3 Plastic rotation according to Eurocode

The simplified method to estimate the rotation capacity of continuous beam or continuous one-way slab is presented in Eurocode 1992-1-1 [13]. The simplified procedure is based on the rotation capacity of beam/slab zones over a length of approximately 1,2 times the depth of section. It is assumed that these zones undergo a plastic deformation (formation of plastic hinges) under the relevant combination of actions. [13].

The recommended values for plastic rotation $\theta_{pl,d}$ as a function of the relative height of the compression zone x_u/d for steel Classes B and C and concrete strength classes less than or equal to C50/60 are presented in Table 5.6N of Eurocode EN 1992-1-1 [13]. In the simplified procedure, the allowable plastic rotation may be determined by multiplying the basic value of allowable rotation, $\theta_{pl,d}$, with a correction factor k_λ that depends on the shear slenderness.

$$k_\lambda = \sqrt{\lambda/3} \tag{15}$$

The values in Eurocode Table 5.6N apply for a shear slenderness $\lambda = 3{,}0$. As a simplification λ may be calculated for the concordant design values of the bending moment M_{sd} and shear V_{sd}

$$\lambda = \frac{M_{sd}}{V_{sd} \cdot d} \tag{16}$$

where d is effective height of the cross-section.

4. EXPERIMENTAL RESULTS AND DISCUSSION

As illustrated in Figures 11 to 14, the rotation of the centre support of the test beams is demonstrated in relation to the total external load. The continuous lines in the figures represent the values obtained from experimental results. The maximum rotation has been obtained mainly through the curvature results and the plastic hinge input. The rotation measurement on both sides of the centre support gave results that were approximately analogous to those obtained through curvature until all plastic hinge regions had been formed on support and mid-spans. The steel bars at the top of the beam on the centre support began to yield at a load level of approximately 800 kN. Another inflection point was observed at the external load level of approximately 1100 kN. At this point, the non-prestressed reinforcement at the midspans reached its yield stress, leading to the formation of all three plastic hinge regions [12]. After this, the aforementioned curves diverged to a minor extent, yet ultimately converged to very similar values, particularly for beams B2 and B3. In beam B4, the torsional load exerts an influence on the rotation in the centre support region.

The various calculation methods have been illustrated in Figures 11 to 14 with dashed lines. The rotation of the centre support, as outlined in the beginning of Section 3.2, has been calculated utilising different values for the bending stiffness. Furthermore, the results obtained from load tests have been utilised in all methods.

Method A – The constant value of elastic bending stiffness $E_{cm}I_g$ was used. The method involved the utilisation of the applied loads and the centre support moments derived from the measurement data of the load sensors of the bearings and the hydraulic jacks.
Method B – The constant value of effective bending stiffness $E_{cm}I_e$ was used. The information from the measurement data, as utilised in method A, has been employed here as well. Furthermore, the effective prestress σ_{pe}, the cracking moment M_{cr} and the total applied moment M_n values from the test data have been utilised in the calculation of the effective bending stiffness.
Method C – The variable values of constant bending stiffness EI were used. The data from the load sensors of the bearings and the hydraulic jacks, as in method A, have been utilised. The determination of the bending stiffness was achieved through the utilisation of measured deflection values in both mid-spans at each load step, as presented in Section 3.1. The changing values are demonstrated in Figure 7.
Method D – The constant value of bending stiffness $E_{cm}I$ calculated from the deflection data of the first load step was used. The measured deflections were utilised to determine additional deflection and rotation, as presented in Chapter 3.2. The data from the load sensors of the bearings and the hydraulic jacks have been utilised in a similar manner to that employed in methods A, B and C.
Method E – The variable values of constant bending stiffness were determined by multiplying the elastic bending stiffness value by the stiffness factors $E_{cm}I_g{\cdot}SF$. The centre support rotation has been calculated in the same way as in methods A, B and C. In the calculation of the stiffness factors for the different load levels, the maximum support moment of the load tests has been used as the bending moment capacity.

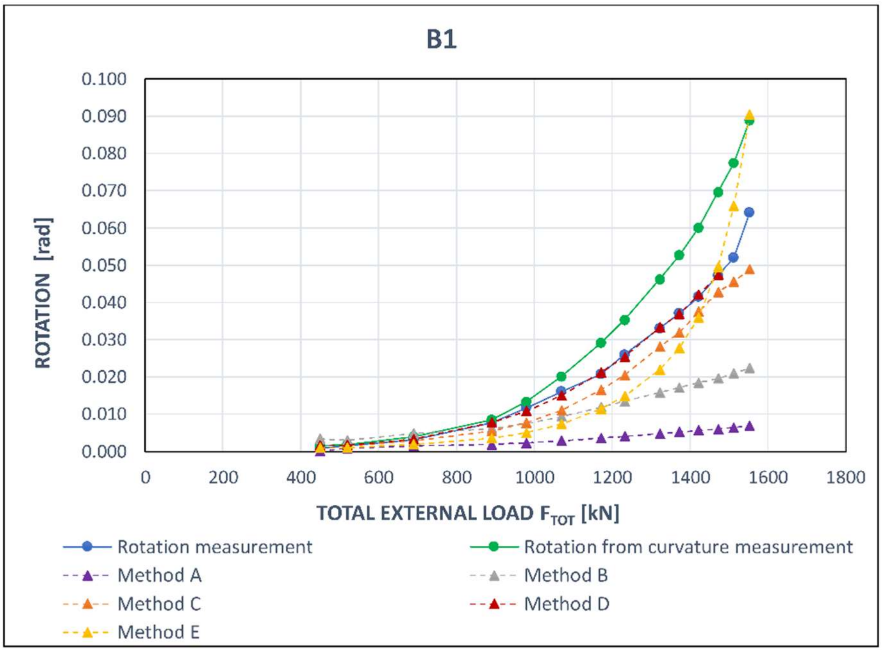

Figure 11 – The rotation of the centre support of beam B1.

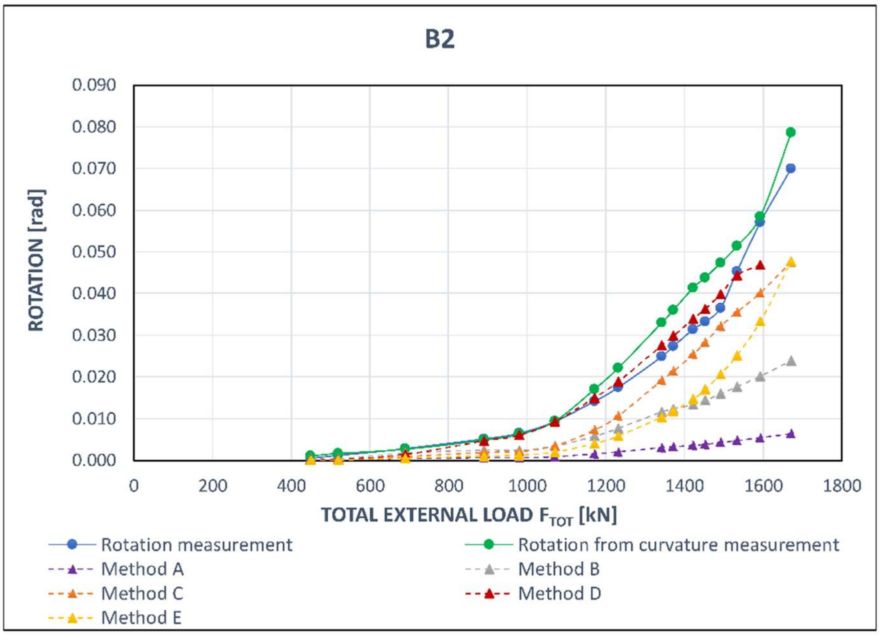

Figure 12 – The rotation of the centre support of beam B2.

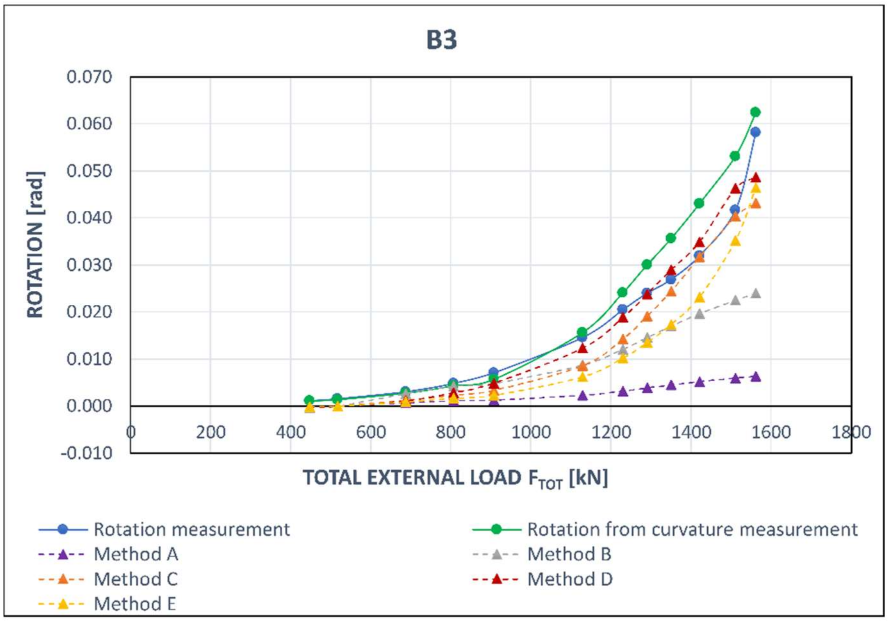

Figure 13 – The rotation of the centre support of beam B3.

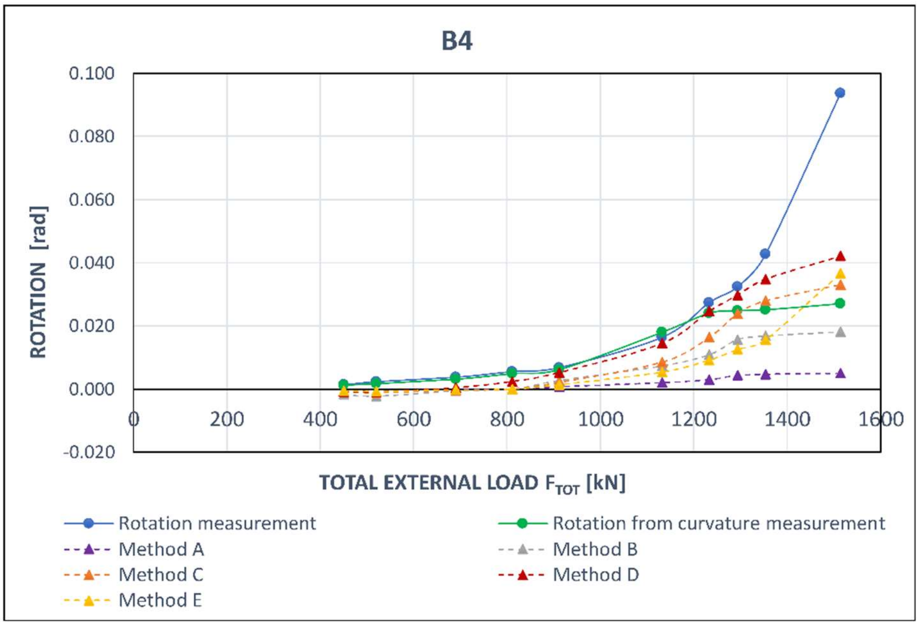

Figure 14 – The rotation of the centre support of beam B4.

A rotation that was fully elastic (method A), with the elastic bending stiffness being utilised in the calculation, gave the smallest total rotation. Furthermore, the rotation was calculated using the superposition principle for the hyperstatic beam, as described in the previous Chapter, and the constant value of the effective stiffness for the bending stiffness along the entire beam (method B). This resulted in rotation values that were evidently larger than those of the elastic curve. The most accurate approximation to the test results was obtained with curves from methods C and D, which were calculated using the methods described in the previous chapter. The method D corresponded well with the rotation result from test beams at all loading levels. The curve that employed the stiffness factor and the elastic bending stiffness (method E) gave results that were highly comparable to the curves from methods C and D at high loading levels but underestimated the reduction in bending stiffness at lower load levels.

In the computational determination of the rotation curves, it is assumed that the bending stiffness is distributed uniformly over the entire length of the beam and its value has decreased. Furthermore, experimental evidence indicates that the bending stiffness has decreased even further at the plastic hinge regions where the formed cracks have been concentrated. Consequently, the calculated curves lie mainly below the experimental results. The utilisation of the effective bending stiffness in the calculation of the rotation curves resulted in outcomes that were too large at the low load steps, as the effective bending stiffness value is smaller than the actual measured values.

The plastic rotation is defined as the rotation that has been formed after the top reinforcement bars have yielded in the support area. In this instance, it can be conceptualised as the discrepancy between the rotation outcome derived from experimental findings (rotation and curvature measurements) and the calculated elastic rotation (method A). Furthermore, the plastic rotation has been calculated from the test results up to the load level at which a compression of 3.5‰ was achieved on the bottom surface of the centre support. This load level was around 1200 kN to 1400 kN. For the comparison, the plastic rotation values were also calculated using methods B, C and D. Methods C and D were used up to the load level at which a compression of 3.5‰ was achieved at the bottom surface. The plastic rotation values of the test beams are illustrated in Figure 15. As demonstrated in test beam B3, which had compression reinforcement at the centre support, a compression of 3.0‰ was only achieved at the end of the load test.

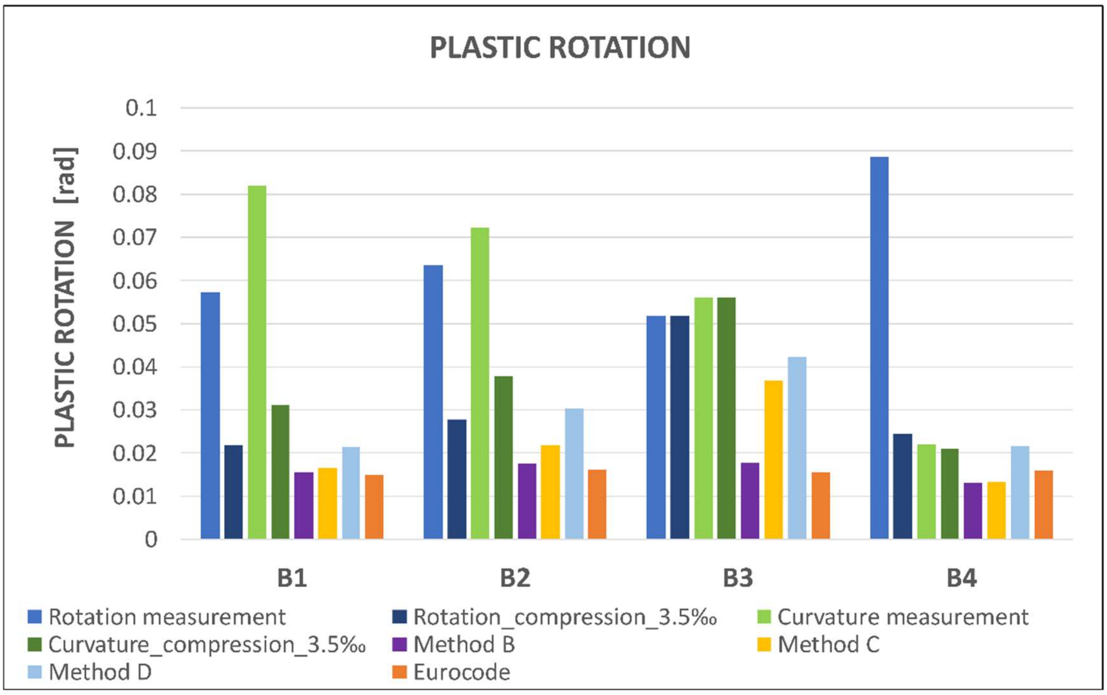

Figure 15 – Plastic rotation of the test beams.

The same figure also shows the values of plastic rotation determined using the Eurocode formulas. The Eurocode estimate appears to be less than approximately one-third of the measured plastic rotation. The difference between the maximum rotation calculated using the effective bending stiffness (method B) and the elastic rotation (method A) is of the same order of magnitude as the plastic rotation capacity according to the Eurocode, around 0.013 to 0.018 1/rad. The plastic rotation values obtained from test results and calculation methods B, C and D, as well as the plastic rotational capacity determined using the Eurocode, exhibited a good degree of correlation with each other when evaluated up to the level of 3.5‰ on the compression fibre. Beam B3 is an exception here due to the compression reinforcement.

5. CONCLUSIONS

Four continuous two-span concrete beams, prestressed with unbonded tendons, were constructed and loaded up to failure at the laboratory of Civil Engineering at Tampere University. All test beams were subjected to bending and shear, with one additionally subjected to torque. This article focuses on the study of the bending stiffness of the test beams and rotation of the centre support. The rotation as a function of total external load has been determined in several different ways. Moreover, a comparison has been made between the magnitude of plastic rotation and the rotational capacity as determined by the Eurocode. The following conclusions have been reached:

- The average bending stiffness $E_{cm}I$, as determined through the measured deflections of the test beams, was clearly less than the calculated elastic value $E_{cm}I_g$, even at the first loading step (serviceability limit state load). The drop was around 100 MNm^2.

- Utilising the stiffness factor (SF) together with the elastic bending stiffness $E_{cm}I$ resulted in a rotation value at high loading levels that is nearly equivalent to that calculated through the use of deflection results, except in beam B1. The SF method may underestimate the reduction in stiffness at lower load levels. Nevertheless, the method is to be considered highly advantageous in instances where the structure is subjected to its maximum capacity and can be employed for design purposes.

- The calculated values of bending stiffness and rotation at the centre support area, as determined by measured deflection, demonstrate a strong correlation with the experimental results, although they remain below the observed values. This is due to the fact that, in the plastic hinge regions, the stiffness undergoes a more rapid decrease.

- The discrepancy between the rotation calculated using the effective bending stiffness and the rotation calculated using the elastic bending stiffness was of the same order of magnitude as the plastic rotation capacity calculated using the Eurocode. The values calculated using methods C and D were found to be in close agreement with those calculated using the Eurocode when plastic rotation was calculated up to the load level at which a compression of 3.5‰ was achieved on the bottom surface of the support. The plastic rotation obtained from measurement results was approximately three times the plastic rotation capacity calculated using the Eurocode.

REFERENCES:

1. Kim, S. K. & Lee, D. H.: ”Nonlinear Analysis Method for Continuous Post-Tensioned Concrete Members with Unbonded Tendons”. *Engineering Structures*, 40, 2012, pp. 487-500
2. Vu N A, Castel A & François R: ”Response of Post-tensioned Concrete Beams with Unbonded Tendons including Serviceability and Ultimate State”. *Engineering Structures*, 32(2), 2010, pp. 556-559
3. Lou T., Lopes S. M.R., Lopes A. V. ”Nonlinear and time-dependent analysis of continuous unbonded prestressed concrete beams”. *Computers and Structures*, 119, 2013, pp. 166-176
4. Moreira L. S., Sousa Jr. J. B. M., Parente Jr. E., ”Nonlinear finite element simulation of unbonded prestressed concrete beams”. *Engineering Structures*, 170, 2018, pp. 167-177
5. Kang T. H.-K., Huang Y., Shin M., Lee J. D., Cho A. S., ”Experimental and Numerical Assessment of Bonded and Unbonded Post-tensioned Concrete Members”. *ACI Structural Journal*, V. 112, No 6, November-December, 2015, pp. 735-748
6. Du J.S., Au F. T.K., Cheung Y.K., Kwan A. K.H., ”Ductility analysis of prestressed concrete beams with unbonded tendons”. *Engineering Structures*, 30, 2008, pp. 13-21
7. Du J.S, Au F. T.K., Chan E. K.H., Liu L., ”Deflection of unbonded partially prestressed concrete continuous beams”. *Engineering Structures*, 118, 2016, pp. 89-96
8. Shaikh AF, Branson DE., ”Non-tensioned steel in prestressed concrete beams”. *PCI Journal* 1970;15(1), pp. 14–36.
9. Terán-Torres, B. T., Elías-Chávez, A. A., Valdez-Tamez, P. L., Rodrígues- Rodrígues., J. A., Juárez-Alvarado, C. A., ”Flexural Stiffness and Crack Width of Partially Prestressed Beams with Unbonded Tendons”. *Buildings*, 13, 2023, pp. 1-27
10. Fu C., Zhu Y., Wang Y., ”Stiffness assessment of cracked post-tensioned concrete beams with unbonded tendons based on the cracking pattern”. *Engineering Structures,* 214, 2020, pp. 1-11
11. Nakari T., Tulonen J., Asp O., Kytölä U., Laaksonen A.: ”Experimental study of moment redistribution in continuous concrete beams prestressed with unbonded tendons”. *Structural Concrete*. 25(4), 2024. pp. 1-18
12. Nakari T., Tulonen J., Laaksonen A.: ”Experimental study of stress increase of unbonded tendons in continuous post-tensioned concrete beams”. *Structural Concrete*. 2025. pp. 1-16
13. European standard EN 1992-1-1, Eurocode 2: Design of concrete structures – Part 1-1: General rules and rules for buildings, 2005, 226 pp.
14. European standard EN 1990, Eurocode – Basis of structural design, 2002, 120 pp.